

## Calculation of Boozer magnetic coordinates for multiple plasma regions (with either closed or open flux surfaces) connected by magnetic separatrices

F. Alladio,<sup>a)</sup> A. Mancuso, and P. Micozzi

Associazione EURATOM-ENEA sulla Fusione, CR Frascati, C.P. 65-00044, Frascati, Rome, Italy

F. Rogier

ONERA-CERT/DTIM/M2SN 2, avenue Edouard Belin-BP 4025-31055, Toulouse Cedex 4, France

(Received 7 June 2005; accepted 26 September 2005; published online 2 November 2005)

Magnetic coordinates ( $\psi_T$ =radial label of flux surfaces,  $\theta$ =poloidal, and  $\phi$ =toroidal angle) are introduced in toroidal magnetoplasma equilibria in order to straighten the field lines [described by:  $\theta - \epsilon(\psi_T)\phi = \text{constant}$  on any flux surface,  $\epsilon(\psi_T)$  being the rotational transform]. The simplest method for analyzing the ideal magnetohydrodynamic (MHD) stability expands the perturbed plasma displacement  $\vec{\xi}$  in magnetic coordinates and solves the normal mode equation through one-dimensional (1D) radial finite elements. This paper extends the calculation of ( Boozer) magnetic coordinates to simply connected equilibria that embed a magnetic separatrix, with regular  $X$ -points ( $\vec{B} \neq 0$ ), and reach the symmetry axis, with singular magnetic  $X$ -points ( $\vec{B} = 0$ ). These configurations include multiple plasma regions, whose outermost one (surrounding plasma) is not composed by toroidal surfaces closed around a single magnetic axis. Two examples are chosen: (i) flux-core-spheromak (FCS) configurations, where the surrounding plasma is a screw pinch, with open flux surfaces; (ii) Chandrasekhar–Kendall–Furth (CKF) configurations, where it is a toroidal shell, carved by multiple toroidal plasma regions. This paper shows that a proper ordering of the radial coordinate  $\psi_T$ , the requirement of continuity for  $\theta$  and  $\phi$  and an  $\epsilon$  matching condition (between neighboring mesh points on opposite sides of the connecting separatrix) resolve the ambiguities in the definition of magnetic coordinates in both CKF and FCS cases. However, a few metric coefficients diverge at the separatrices; therefore, often numerical MHD stability codes do not use magnetic coordinates there, but adopt local two-dimensional (2D) finite elements. This paper instead investigates all the divergences, in order to allow for the asymptotic analysis of  $\vec{\xi}$  near the separatrices, with the purpose of maintaining the magnetic coordinate method and the 1D radial finite elements in the ideal MHD stability analysis. © 2005 American Institute of Physics.

[DOI: 10.1063/1.2122487]

### I. INTRODUCTION

The spherical tokamaks with aspect ratio  $A = R_0/a < 2$  ( $R_0$ =torus major radius,  $a$ =torus minor radius) were originally proposed<sup>1</sup> in the 1980s and have led in 20 years time to a number of very successful concept exploration<sup>2</sup> and proof of principle<sup>3,4</sup> experiments. In view of a magnetic fusion reactor, the low aspect ratio, meaning low volume and low cost, should provide economical advantages as well as attractive features for the physics such as: High plasma beta, mitigated disruptions and low geodesic curvature of the magnetic field lines. A central post, containing the inner part of the toroidal magnet, links the plasma torus; upon decreasing the aspect ratio down to  $A < 1.3$  it is possible to obtain magnetohydrodynamic (MHD) equilibria<sup>5</sup> with a higher ratio between the current in the toroidal plasma ( $I_{ST}$ ) and the current in the centerpost ( $I_{CP}$ ),  $I_{ST}/I_{CP} \geq 1$ . However, the very limited space left for the centerpost at  $A < 1.3$ , cannot host a conventional ohmic transformer and, therefore, need noninductive current drive methods for plasma start-up, ramp-up, and sus-

tainment. Another problem is that the centerpost cannot be shielded from the neutron flux and therefore cannot be a superconductor.

Moving from these configurations, the Frascati-ENEA research center has completed the design study of a novel compact torus, Spherical Plasma for Helicity Relaxation Assessment (PROTO-SPHERA),<sup>6</sup> in which a force-free screw pinch (SP, carrying a total poloidal plasma current  $I_e$ ), fed by electrodes, will be employed in place of a metal centerpost. The SP will be surrounded by a spherical torus [ST carrying a total toroidal plasma current  $I_{ST}$ , see Fig. 1(a)], with closed flux surfaces and with a rather large volume averaged plasma beta:  $\beta_{ST} = 2\mu_0 \langle p \rangle_{ST} / \langle B^2 \rangle_{ST} \approx 0.15 - 0.2$ . The SP and the ST will have a common embedded magnetic separatrix: Magnetic reconnections will occur at the regular  $X$ -points ( $\vec{B} \neq 0$ ), injecting magnetic helicity, poloidal flux and plasma current from the electrode-driven SP into the ST and converting into plasma kinetic energy a fraction of the injected magnetic energy. The SP will be magnetically given a mushroom-shape near each electrode, with a singular magnetic  $X$ -point ( $\vec{B} = 0$ ) on the symmetry axis. Such a configu-

<sup>a)</sup>Electronic mail: alladio@frascati.enea.it

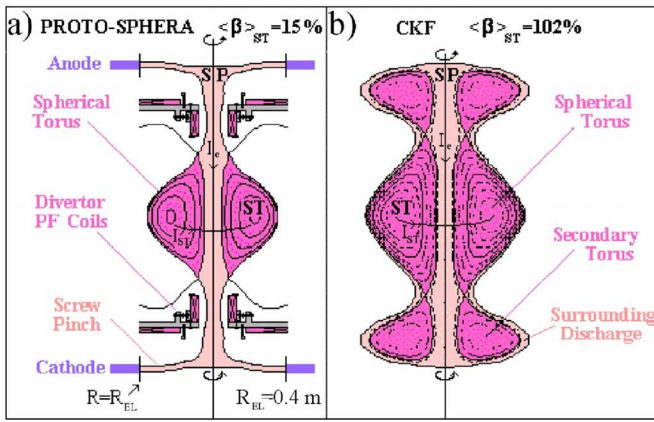


FIG. 1. (Color online). Comparison between: (a) PROTO-SPHERA; (b) a CKF configuration.

ration was devised theoretically under the name “bumpy Z pinch”<sup>7</sup> or “flux-core-spheromak”<sup>8</sup> (FCS) and was then studied experimentally in the Flux Amplification Compact Toroid (FACT)<sup>9</sup> and Tokyo University Spherical Torus No. 3 (TS-3)<sup>10</sup> experiments. However, the resistivity of a SP plasma centerpost should always remain larger than the resistivity of a corresponding copper centerpost, unless a plasma electron temperature  $T_e^{\text{pinch}} \approx 700 \text{ eV}$  is achieved, which seems incompatible with open flux surface fed by electrodes. As a consequence, in a fusion reactor a plasma centerpost would dissipate too much energy compared with the fusion energy output. A plasma centerpost reactor extrapolation could instead be a generalization of the FCS configurations, in which the plasma is initiated by electrodes but is then sustained in absence of electrodes; an example of such configurations are the Chandrasekhar–Kendall–Furth (CKF) equilibria<sup>11</sup> [see Fig. 1(b)]. They embed a magnetic separatrix, with regular X-points ( $\vec{B} \neq 0$ ), dividing a main spherical torus (ST), two secondary tori (SC) on top and bottom and a plasma discharge (SP) surrounding the three tori; furthermore two singular magnetic X-points ( $\vec{B} = 0$ ) are present on the symmetry axis. Comparing Fig. 1(b) with Fig. 1(a) it is evident that the CKF surrounding plasma replaces the FCS force-free screw pinch in the inboard, whereas the secondary tori replace the FCS divertor poloidal field coils.

The matching of multiple plasma configurations, even including, like in FCS, open and closed flux-surfaces, brings to life several radically new issues. The equilibrium of such combined systems has already been analyzed,<sup>12,13</sup> under the assumption that (singular) surface current density is absent on the magnetic separatrices; the kinetic plasma pressure  $p(\psi)$  and the normalized poloidal plasma current  $f(\psi) = RB_\phi$  (where  $B_\phi$  is the toroidal field at a distance  $R$  from the symmetry axis) are, therefore, continuous at the magnetic separatrices, whereas the total plasma current density  $\vec{j}$  may have jumps there. The computation of the ideal MHD stability requires instead new developments. In the case of CKF configurations: (i) A magnetic separatrix defines the interface between the different plasma regions; (ii) the presence of multiple plasma regions with closed flux surfaces surrounding multiple magnetic axes must be correctly accounted for.

The ideal MHD stability of the combined system is studied by solving the eigenvalue problem:<sup>14</sup>

$$\vec{W} \cdot \vec{\xi} = \omega^2 \vec{K} \cdot \vec{\xi}, \quad (1)$$

where  $\vec{W}$  is the plasma perturbed potential energy and  $\vec{K}$  the plasma perturbed kinetic energy, associated with the perturbed plasma displacement  $\vec{\xi}$ . The use of magnetic coordinates, in which field lines are straight, defines the simplest approach to the numerical study of the ideal MHD stability of magnetoplasma equilibria: It allows the use of one-dimensional radial finite elements, while adopting a Fourier decomposition in the poloidal angle. However, the magnetic coordinates become singular in presence of magnetic separatrices. In order to avoid these singularities some ideal MHD stability codes<sup>15</sup> have adopted 2D finite elements, still aligned with the flux surfaces, either all over the mesh or just near the magnetic separatrix. The approach taken here is instead that of maintaining the 1D radial finite elements and of using the asymptotic analysis of the perturbed plasma displacement near the separatrices: The logarithmic dependence of the rotational transform  $\iota$  imposes asymptotic limits to the perturbed plasma displacement  $\vec{\xi}$  for low toroidal mode number ( $n=0-3$ ) global MHD perturbations near the embedded separatrix, while the vanishing of  $\vec{B}$  at the singular X-points plays the same role for the outer separatrix.

In the case of flux-core-spheromaks: (i) A magnetic separatrix defines the interface between the different plasma regions; (ii) the combined configuration composed by the ST, with closed flux surfaces, and by the SP, with open flux surfaces ending upon electrodes, must be correctly modeled. The definitions of the magnetic coordinates on open flux surfaces is ambiguous, due to the absence of well defined periodicities: This paper solves the ambiguity through the choices that are most suitable for the computation of the ideal MHD stability. Apart from the specific application presented in this paper, the method of calculating magnetic coordinates on combined plasmas with closed and open flux surfaces can find applications to any separatrix-limited toroidal configurations, when a current is driven along the open flux surfaces (biased divertors and coaxial helicity injection in conventional and spherical tokamaks).

The calculation of the magnetic Boozer coordinates on axisymmetric plasma equilibria with the topology of a torus is briefly reviewed in Sec. II. The ordering of the radial coordinate  $\psi_r$  for CKF configurations is presented in Sec. III. The calculation of the coordinates inside the secondary tori meets problems for the continuity of the angles  $\theta$  and  $\phi$  as well as for the nonorthogonality coefficient  $\beta_*$ ; these problems are solved in Sec. IV. Section V discusses the Boozer coordinates for the whole CKF equilibrium, their correspondence between the tori and the surrounding plasma and their mirroring between the lower and the upper SC tori. Thereafter the metric coefficients are written down and their singularities near magnetic separatrices are analyzed in Sec. VI. Section VII switches to the FCS configurations, considers the requirements which must be met to extend the calculation of the Boozer coordinates to open flux surfaces and details such

calculation near the magnetic separatrix. Section VIII extends the calculation to all open flux surfaces, up to the symmetry axis. Conclusions are summarized in Sec. IX.

## II. BOOZER COORDINATES FOR AXISYMMETRIC TORI

Axisymmetric MHD equilibrium calculations are usually carried out in terms of the poloidal flux enclosed within each magnetic surface:

$$\psi = \int \vec{\mathbf{B}} \cdot d\vec{\mathbf{S}}_p. \quad (2)$$

For toroidal plasmas (doubly connected plasma regions with toroidal magnetic surfaces closed around a single magnetic axis), the poloidal flux is  $\psi=0$  on the symmetry axis (where no plasma is present),  $\psi=\psi_{\text{edge}}$  at the plasma edge and  $\psi=\psi_{\text{max}}$  at the magnetic axis. The use of nonorthogonal periodical Boozer coordinates<sup>16</sup> ( $\psi_T$ =radial coordinate,  $\theta$ =poloidal angle,  $\phi$ =toroidal angle, not coincident with the geometric azimuth  $\varphi$ , with  $\vec{\nabla}\varphi=\hat{\mathbf{e}}_\varphi/R$ , where  $\hat{\mathbf{e}}_\varphi$  is the unit vector along the geometric azimuth) simplifies<sup>17,18</sup> the calculation of the ideal MHD stability. In particular Boozer coordinates are chosen as they minimize<sup>19</sup> the number of Fourier terms in the poloidal angle decomposition of the perturbed plasma displacement  $\vec{\xi}$ . The radial coordinate is the normalized toroidal flux within each magnetic surface:

$$\psi_T(\psi) = \frac{1}{2\pi} \int \vec{\mathbf{B}} \cdot d\vec{\mathbf{S}}_T, \quad (3)$$

with  $\psi_T=0$  on the magnetic axis and  $\psi_T=\psi_T^{\text{edge}}$  at the plasma edge. Other quantities must be introduced such as the normalized poloidal flux:

$$\psi_p(\psi_T) = \frac{1}{2\pi} \int \vec{\mathbf{B}} \cdot d\vec{\mathbf{S}}_p = \psi/2\pi, \quad (4)$$

the rotational transform, which is the inverse of the MHD safety factor  $q$ :

$$\epsilon(\psi_T) = -d\psi_p/d\psi_T, \quad (5)$$

the normalized toroidal current, defined from the total toroidal current  $I_\varphi$ :

$$I(\psi_T) = \frac{1}{2\pi} \int \vec{\nabla} \wedge \vec{\mathbf{B}} \cdot d\vec{\mathbf{S}}_T = \mu_0 I_\varphi(\psi_T)/2\pi, \quad (6)$$

and the normalized poloidal current, defined from the total poloidal current  $I_{\text{dia}}$ :

$$f(\psi_T) = \frac{1}{2\pi} \int \vec{\nabla} \wedge \vec{\mathbf{B}} \cdot d\vec{\mathbf{S}}_p = \mu_0 I_{\text{dia}}(\psi_T)/2\pi = RB_\varphi. \quad (7)$$

The magnetic field in terms of the contravariant basis vectors  $\vec{\nabla}\psi_T$ ,  $\vec{\nabla}\theta$ ,  $\vec{\nabla}\phi$  is

$$\vec{\mathbf{B}} = \beta_* \vec{\nabla}\psi_T + I \vec{\nabla}\theta + f \vec{\nabla}\phi, \quad (8)$$

with  $B_\psi = \beta_*(\psi_T, \theta)$ ,  $B_\theta = I(\psi_T)$ ,  $B_\phi = f(\psi_T)$ , as covariant components.

When expressed in terms of the covariant basis vectors:<sup>20</sup>

$$\vec{\mathbf{e}}_\psi = \sqrt{g} \vec{\nabla}\theta \wedge \vec{\nabla}\phi, \quad \vec{\mathbf{e}}_\theta = \sqrt{g} \vec{\nabla}\phi \wedge \vec{\nabla}\psi_T, \quad (9)$$

$$\vec{\mathbf{e}}_\phi = \sqrt{g} \vec{\nabla}\psi_T \wedge \vec{\nabla}\theta,$$

the magnetic field is

$$\vec{\mathbf{B}} = (\epsilon/\sqrt{g}) \vec{\mathbf{e}}_\theta + (1/\sqrt{g}) \vec{\mathbf{e}}_\phi = \vec{\nabla}\psi_T \wedge (\vec{\nabla}\theta - \epsilon \vec{\nabla}\phi), \quad (10)$$

with  $B^\psi=0$ ,  $B^\theta = \epsilon/\sqrt{g}$ ,  $B^\phi = 1/\sqrt{g}$  as contravariant components and the Jacobian:

$$\sqrt{g} = [\vec{\nabla}\psi_T \cdot (\vec{\nabla}\theta \wedge \vec{\nabla}\phi)]^{-1} = [f(\psi_T) + \epsilon(\psi_T)I(\psi_T)]/B^2. \quad (11)$$

The equilibrium condition  $\vec{\nabla}p = \vec{\mathbf{j}} \wedge \vec{\mathbf{B}}$  becomes<sup>17</sup> in axisymmetry

$$\mu_0 \sqrt{g} (dp/d\psi_T) + (df/d\psi_T + \epsilon dI/d\psi_T) = \epsilon \partial \beta_* / \partial \theta. \quad (12)$$

The variable part of this equation is the differential expression of the nonorthogonality coefficient  $\beta_*(\psi_T, \theta)$ :

$$\epsilon \partial \beta_* / \partial \theta = \mu_0 (dp/d\psi_T) \left[ \sqrt{g} - \oint d\theta \sqrt{g} / 2\pi \right]. \quad (13)$$

Alternative choices for magnetic coordinates have been considered, among those already used in other MHD stability analysis. In particular the Princeton Equilibrium, Stability, and Transport code (PEST-1) coordinates<sup>21</sup> [with  $\sqrt{g_{\text{PEST-1}}} \propto R^2/f(\psi)$ ] have the advantage that the toroidal angle coincides with the geometric azimuth  $\varphi$ , but are better avoided for plasma configurations extending up to the symmetry axis, as an artificial singularity  $1/R$  would be introduced upon the gradient  $\vec{\nabla}\psi_{\text{PEST-1}}$  of its radial coordinate ( $\psi_{\text{PEST-1}} \propto \int d\psi/f(\psi)$ ). A valid alternative to the Boozer coordinates would have been that of the Hamada coordinates<sup>22</sup> (with  $\sqrt{g_H}=1$ ), but also in this case the toroidal angle  $\phi_H$  would not coincide with the geometric azimuth  $\varphi$ . In an axisymmetric toroidal MHD plasma equilibrium, which is calculated having as inputs  $p(\psi)$ ,  $f(\psi)$  and the total toroidal current  $I_\varphi(\psi_{\text{edge}})$  at the plasma edge, the magnetic field is decomposed into the toroidal and poloidal components as:  $\vec{\mathbf{B}} = B_p \hat{\mathbf{e}}_p + f(\psi) \vec{\nabla}\varphi$  and the method for deriving the periodical Boozer coordinates can be so summarized:

- The rotational transform is<sup>23</sup>

$$\epsilon(\psi) = \frac{2\pi}{f(\psi) \oint \frac{1}{R^2 B_p} \hat{\mathbf{e}}_p \cdot d\vec{\mathbf{l}}_p}, \quad (14)$$

$\hat{\mathbf{e}}_p$  being the poloidal unit vector and  $d\vec{\mathbf{l}}_p$  the differential arc-length.

- The radial coordinate is calculated through (5):

$$\psi_T = -\frac{1}{2\pi} \int_{\psi_{\text{max}}}^{\psi} \frac{d\psi}{\epsilon(\psi)}. \quad (15)$$

- The first non-periodical Boozer coordinate<sup>16</sup>  $\theta_0$ , with  $\theta_0 = \theta - \epsilon\phi$ , is evaluated from  $\vec{\mathbf{B}} = \vec{\nabla}\psi_T \wedge \vec{\nabla}\theta_0$  as

$$\theta_0(s) = \epsilon(\psi_T) f(\psi_T) \int_0^s \frac{1}{R^2 B_p} \hat{\mathbf{e}}_p \cdot d\vec{\mathbf{l}}_p - \epsilon(\psi_T) \varphi, \quad (16)$$

with  $\theta_0=0$  on all flux surfaces at the outboard of the torus ( $s=0$ ), at the geometrical azimuth  $\varphi=0$  [gauge invariance of  $\theta_0$ :  $\hat{\theta}_0 = \theta_0 + \theta^*(\psi_T)$ ].

• The second nonperiodical Boozer coordinate<sup>16</sup>  $\chi_0$  ( $d\chi_0 = \vec{\mathbf{B}} \cdot d\vec{\mathbf{l}}$ , where  $d\vec{\mathbf{l}}$  is the differential arc-length along the field line) is evaluated as

$$\chi_0(s) = \int_0^s B_p \hat{\mathbf{e}}_p \cdot d\vec{\mathbf{l}}_p + f(\psi_T) \varphi, \quad (17)$$

with  $\chi_0=0$  on all flux surfaces at the outboard of the torus ( $s=0$ ), at  $\varphi=0$  [gauge invariance of  $\chi_0$ :  $\hat{\chi}_0 = \chi_0 + \chi^*(\psi_T)$ ].

• Then the periodical Boozer angles are calculated as

$$\theta = \frac{\epsilon\chi_0 + f\theta_0}{f + \epsilon I}, \quad \phi = \frac{\chi_0 - I\theta_0}{f + \epsilon I}. \quad (18)$$

If the toroidal plasma is up-down symmetric, then  $\beta_* = 0$  at  $\theta = 0$  for every  $\psi_T$ ; if it is not, a method for integrating  $\beta_*(\psi_T, \theta)$  from (13) will be detailed in Sec. V. In general a force-free plasma ( $\vec{\nabla} p = 0$ ) has  $\beta_* = 0$  everywhere.

### III. ORDERING OF THE RADIAL VARIABLE IN PRESENCE OF MULTIPLE MAGNETIC AXES

As the CKF configurations are mostly composed by multiple axisymmetric toroidal regions (with the exception of the surrounding plasma), the calculation of the Boozer coordinates in each torus is in principle the standard one, just illustrated in the previous section. However, a few corrections must be introduced; they are illustrated in this section and in the following two. The first correction deals with the ordering of the magnetic surfaces, which must account for the multiplicity of magnetic axes, see Fig. 2. The radial variable  $\psi_T$  starts at the magnetic axis of the main ST with  $\psi_T = 0$ , reaches  $\psi_T = \psi_T^X$  on the separatrix, with  $\vec{\nabla} \psi_T$  pointing toward the edge. After that, indicating with  $\psi_T^{SC}$  the normalized toroidal flux included inside each secondary torus, the radial variable  $\psi_T$  reenters the upper SC and runs with  $\vec{\nabla} \psi_T$  pointing inside, reaching  $\psi_T = \psi_T^X + \psi_T^{SC}$  at the magnetic axis of the upper SC. Thereafter the radial variable  $\psi_T$  jumps to the magnetic axis of the lower SC ( $\psi_T = \psi_T^X + \psi_T^{SC}$ ), runs with  $\vec{\nabla} \psi_T$  pointing toward the edge and reaches  $\psi_T = \psi_T^X + 2\psi_T^{SC}$  at the magnetic separatrix. Finally, the radial variable  $\psi_T$  continues through the surrounding plasma and reaches  $\psi_T = \psi_T^{\max}$  at the plasma edge and on the symmetry axis ( $R=0$ ).

If the up-down symmetry is removed the two SCs will have a different poloidal flux, with only the SC at larger  $\psi$  joined by a first common embedded separatrix to the main ST and with the surrounding plasma divided in two by a second embedded separatrix, which will join only with the SC at smaller  $\psi$ . The ordering of the radial variable will then be slightly changed, with the innermost surrounding plasma

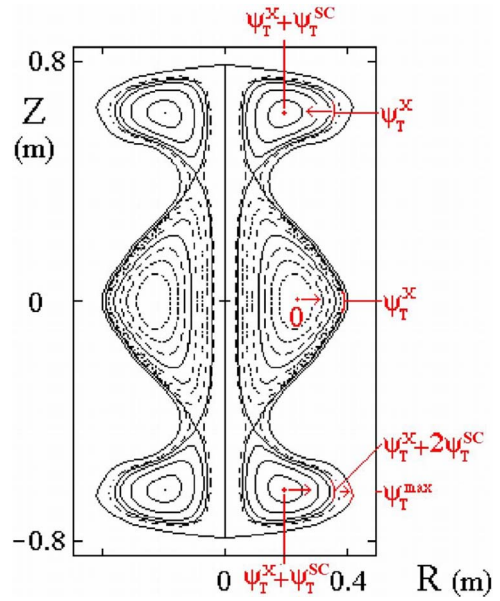


FIG. 2. (Color online). Ordering of the radial variable  $\psi_T$  for an unrelaxed CKF configuration with high plasma beta inside the ST:  $\langle \beta \rangle_{ST} = 1.02$ . The arrows indicate the direction of  $\vec{\nabla} \psi_T$ .

run through twice (with opposite directions of  $\vec{\nabla} \psi_T$ ) before running (again with opposite directions of  $\vec{\nabla} \psi_T$ ) into the two different up-down asymmetric SCs.

### IV. BOOZER COORDINATES INSIDE THE SECONDARY TORI

In the CKF configurations the calculation of the Boozer coordinates inside the secondary tori meets furthermore the problem that additive constants must be fixed: In the calculation of  $\theta$ , in the calculation of the deviation between  $\phi$  and the geometrical azimuth [ $\nu(\psi, \theta) = \phi - \varphi$ ]; and, finally, in the calculation of  $\beta_*(\psi, \theta)$ . On the outermost magnetic surface of the ST ( $\psi = \psi_X + \epsilon_{ST}$ ) the poloidal angle is  $\theta = \theta_X$  at the point with the smallest vertical ( $Z$ ) coordinate. The obvious choice of continuity is to fix  $\theta = \theta_X$  on the outermost magnetic surface of the lower SC ( $\psi = \psi_X + \epsilon_{SC}$ ) at the point with the largest vertical coordinate. This fixes  $\theta = \theta^0$  on the outermost magnetic surface of the lower SC, at the point that has the same vertical coordinate as the magnetic axis (see Fig. 3). The gauge invariance<sup>16</sup> of Boozer coordinates,  $\hat{\theta} = \theta + \theta^*(\psi)$ , is used by fixing  $\theta = \theta^0$  upon the curve normal to the SC magnetic surfaces

$$\vec{\nabla} \psi_T \cdot \vec{\nabla} \theta|_{\theta = \theta^0} = 0, \quad (19)$$

which starts from the point  $(\psi_X + \epsilon_{SC}, \theta^0)$ , see Fig. 3. The poloidal angle  $\theta$  is, therefore, determined inside the lower SC. The continuity for  $\phi$

$$\phi - \varphi = \nu(\psi_X + \epsilon_{SC}, \theta_X) = \nu(\psi_X + \epsilon_{ST}, \theta_X), \quad (20)$$

is similarly imposed at the point  $\theta = \theta_X$  on the outermost magnetic surface of the lower SC. The gauge invariance<sup>16</sup> of Boozer coordinates,  $\hat{\phi} = \phi + \phi^*(\psi)$ , gives

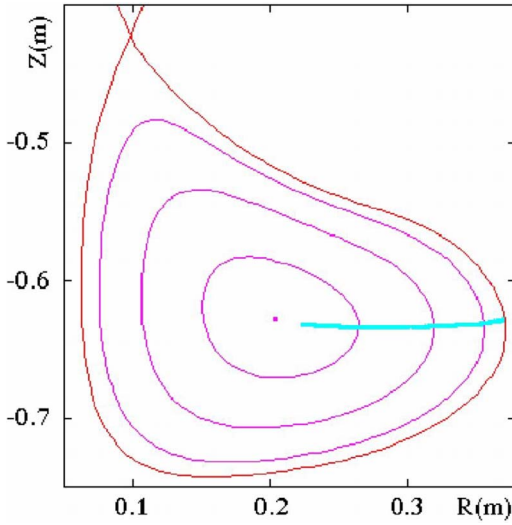


FIG. 3. (Color online). Curve  $\theta = \theta^0$ , normal to flux surfaces, starting from a point on the outermost magnetic surface of the lower SC with the same vertical coordinate as the magnetic axis.

$$\nu(\psi, \theta^0) = \text{constant}, \quad (21)$$

along the same curve  $\theta = \theta^0$ , see Fig. 3, which is then characterized by

$$\partial \nu / \partial \psi_T |_{\theta} = 0. \quad (22)$$

The toroidal angle  $\phi$  is, therefore, determined inside the lower SC. The system between the two equations ( $\vec{\nabla} \psi_T \cdot \vec{\nabla} \phi = 0$ ,  $\vec{\nabla} \psi_T \cdot \vec{\mathbf{B}} = 0$ ) gives

$$\beta_* = -f \frac{\partial \nu}{\partial \psi_T} - \frac{(I + f \partial \nu / \partial \theta)}{|\vec{\nabla} \psi_T|^2} (\vec{\nabla} \theta \cdot \vec{\nabla} \psi_T). \quad (23)$$

As (22) and (19) hold upon the curve  $\theta = \theta^0$ , the additive constant for the nonorthogonality coefficient must be  $\beta_*(\psi_T, \theta^0) = 0$ ; the integration of Eq. (13),

$$\beta_*(\psi, \theta) = 2\pi\mu_0 \left( dp/d\psi \right) \int_{\theta_0}^{\theta} d\theta' \left[ \sqrt{g(\psi, \theta')} \right] - \oint d\theta' \sqrt{g(\psi, \theta') / 2\pi}, \quad (24)$$

determines the nonorthogonality coefficient  $\beta_*$  inside the lower SC.

## V. CORRESPONDENCE OF THE POLOIDAL ANGLE BETWEEN THE TORI AND THE SURROUNDING PLASMA

For the CKF configurations a final problem appears: the correspondence of the poloidal angle between the tori and the surrounding plasma, which is not a toroidal region but, instead, a toroidal shell carved by three toroidal regions. In the ideal MHD stability calculations the normal perturbed plasma displacement variable  $\xi^\psi = \vec{\xi} \cdot \vec{\nabla} \psi_T$  must be continuous<sup>24</sup> at the embedded magnetic separatrix, while the other two displacement variables,  $\eta^\psi = \vec{\xi} \cdot (\vec{\nabla} \theta - \epsilon \vec{\nabla} \phi)$  and  $\mu = -\sqrt{g} \vec{\xi} \cdot \vec{\nabla} \phi$  can be discontinuous. To solve the normal-mode

equation (1) for the ideal MHD stability of an axisymmetric and up-down symmetric plasma equilibrium, the perturbed displacement variables ( $\xi^\psi, \eta^\psi, \mu$ ) are Fourier expanded, labeling each mode by an index  $l$ , corresponding to a poloidal number  $m_l$  and a (fixed as separable) toroidal number  $n$ :

$$\xi^\psi = \sum_l \xi_l(\psi_T) \sin(m_l \theta - n \phi), \quad (25)$$

$$(\eta^\psi, \mu) = \sum_l (\eta_l, \mu_l)(\psi_T) \cos(m_l \theta - n \phi).$$

Numerical accuracy requires that stability calculations based upon 1D finite element method always use an inhomogeneous (intensified) numerical radial mesh near the magnetic separatrices. Along the magnetic separatrix on the side of the three tori, the Boozer poloidal angles can be patched together by allowing jumps of  $2\pi$  inside the main ST, which are admissible due to the Fourier expansion (25) of the perturbed displacement variables: The poloidal angle  $\theta^{\text{ST}}$  makes an excursion  $[0, \theta_X]$  upon the lower outboard of the main ST and then  $\theta^{\text{SC}}$  runs in the range  $[\theta_X, 2\pi + \theta_X]$  around the lower SC;  $\theta^{\text{ST}}$  continues through the range  $[2\pi + \theta_X, 4\pi - \theta_X]$  upon the inboard of the main ST and then  $\theta^{\text{SC}}$  runs in the range  $[4\pi - \theta_X, 6\pi - \theta_X]$  around the upper SC; finally  $\theta^{\text{ST}}$  closes its run in the range  $[6\pi - \theta_X, 6\pi]$  upon the upper outboard of the main ST. On the side of the surrounding plasma, the magnetic angles, labeled by  $\theta^{\text{SP}}$  and  $\phi^{\text{SP}}$ , are calculated in the standard way illustrated in Sec. III (also within the SP each flux surface has a toroidal topology). However, the only possibility for enforcing the continuity of the angle  $\theta$  between the neighboring radial mesh points on opposite sides of the embedded magnetic separatrix is to use inside the SP the multiple of the poloidal angle  $3 \cdot \theta^{\text{SP}}$ , which covers the range  $[0, 6\pi]$  ( $2\pi$  times the number of magnetic axes that carve the toroidal shell). MHD “global” modes must have periodical perturbed displacements (25) over the whole plasma: For these modes the allowed poloidal mode numbers can be all the relative integers  $m_l$  inside the three tori; therefore, the continuity of  $\xi^\psi$  and the correspondence between  $3 \cdot \theta^{\text{SP}}$  and  $(\theta^{\text{ST}}, \theta^{\text{SC}})$  forces the allowed poloidal mode numbers of the global perturbations to be limited to relative integers multiples of 3 inside the SP (a second class of MHD modes with all the relative integers as allowed poloidal mode numbers inside the SP can, however, exist, but they are purely internal to the SP: Their  $\xi^\psi$  vanishes at the embedded separatrix and they must not match any periodicity requirement on the three tori).

The field lines are in correspondence at the ST-SP and at the SC-SP interfaces along the embedded magnetic separatrix; this implies the continuity of the field line labels  $\theta^{\text{ST}} - \epsilon^{\text{ST}}(\psi_T) \phi^{\text{ST}}$ ,  $3\theta^{\text{SP}} - 3\epsilon^{\text{SP}}(\psi_T) \phi^{\text{SP}}$  and  $\theta^{\text{SC}} - \epsilon^{\text{SC}}(\psi_T) \phi^{\text{SC}}$  between neighboring radial mesh points ( $\psi_X + \epsilon_{\text{ST}}, \psi_X - \epsilon_{\text{SP}}, \psi_X + \epsilon_{\text{SC}}$ ) on opposite sides of the embedded magnetic separatrix. The correspondence between  $3 \cdot \theta^{\text{SP}}$  and  $(\theta^{\text{ST}}, \theta^{\text{SC}})$  forces the matching condition for the rotational transform:

$$\epsilon_{\text{CKF}}^{\text{ST}}(\psi_X + \epsilon_{\text{ST}}) = 3 \cdot \epsilon_{\text{CKF}}^{\text{SP}}(\psi_X - \epsilon_{\text{SP}}) = \epsilon_{\text{CKF}}^{\text{SC}}(\psi_X + \epsilon_{\text{SC}}). \quad (26)$$

Appendix A shows that  $\epsilon(\psi)$  near the embedded separatrix exhibits the logarithmic behavior (A1)  $\lim_{\psi \rightarrow \psi_X} \epsilon(\psi) = -A/\ln|C(\psi - \psi_X)|$ . The coefficients  $A$  and  $C$  can be found by a fitting procedure down to the minimum distance from the magnetic separatrix where  $\epsilon(\psi)$  can still be calculated numerically from (14), typically  $|\psi - \psi_X| \approx (1-5) \cdot 10^{-3} \psi_X$ . A characteristic property of the CKF configurations, which depends upon the different values taken by the coefficients  $A$  and  $C$  in the different plasma regions, is that, if  $\epsilon(\psi)$  was calculated at the same distance  $\epsilon_{\text{SP}}$  from all the sides of the embedded separatrix, the rotational transform on the ST and the SC side would be about twice as on the SP side:  $\epsilon_{\text{CKF}}^{\text{ST}}(\psi_X + \epsilon_{\text{SP}}) \approx \epsilon_{\text{CKF}}^{\text{SC}}(\psi_X + \epsilon_{\text{SP}}) \approx 2 \cdot \epsilon_{\text{CKF}}^{\text{SP}}(\psi_X - \epsilon_{\text{SP}})$ , in contradiction with (26). Therefore, given  $\epsilon_{\text{SP}} \approx (1-5) \cdot 10^{-3} \psi_X$ , the matching condition (26) and the logarithmic behavior (A1) are instead used to extrapolate  $\epsilon_{\text{ST}}$  and  $\epsilon_{\text{SC}}$ , to distances smaller than  $\epsilon_{\text{SP}}$ :  $\epsilon_{\text{ST}} \approx \epsilon_{\text{SC}} \approx (2 \cdot 10^{-5} - 10^{-4}) \psi_X$ .

The Boozer coordinates  $\theta$  and  $\phi$ , their nonorthogonality coefficient  $\beta_*$  and their Jacobian  $\sqrt{g}$  are accurately mapped in cylindrical coordinates  $(R, \varphi, Z)$ . For a CKF configuration the mapping consists in a series of 200 Fourier components and in a  $\psi_T$  interpolation with cubic splines, based upon 40 flux surfaces inside the ST, 20 flux surfaces inside each SC and 20 flux surfaces inside the SP:

$$\begin{aligned} R &= \sum_{j=0}^{200} [\delta_j^{R,c}(\psi_T) \cos(-j\theta) + \delta_j^{R,s}(\psi_T) \sin(-j\theta)], \\ Z &= \sum_{j=0}^{200} [\delta_j^{Z,c}(\psi_T) \cos(-j\theta) + \delta_j^{Z,s}(\psi_T) \sin(-j\theta)], \\ \varphi &= \phi + \sum_{j=0}^{200} [\delta_j^{\phi,c}(\psi_T) \cos(-j\theta) + \delta_j^{\phi,s}(\psi_T) \sin(-j\theta)] \\ &= \phi - \nu(\psi_T, \theta), \\ B^2 &= \sum_{j=0}^{200} [\delta_j^{B,c}(\psi_T) \cos(-j\theta) + \delta_j^{B,s}(\psi_T) \sin(-j\theta)], \\ \beta_* &= \sum_{j=0}^{200} [\delta_j^{\beta,c}(\psi_T) \cos(-j\theta) + \delta_j^{\beta,s}(\psi_T) \sin(-j\theta)]. \end{aligned} \quad (27)$$

The relaxation parameter  $\mu = \mu_0(\vec{j} \cdot \vec{B})/B^2$  and the vector  $\vec{\nabla}\psi_T$  are also mapped in cylindrical coordinates through series expansions of the same kind as (27). The Boozer coordinates  $\psi_T$  and  $\theta$  are shown upon the poloidal plane in Fig. 4, with the poloidal angle labeled by  $3 \cdot \theta^{\text{SP}}$  inside the SP. However, the correspondence between  $3 \cdot \theta^{\text{SP}}$  and  $(\theta^{\text{ST}}, \theta^{\text{SC}})$  does not show up clearly in the global equilibrium plot of Fig. 4. This is due to the fact that the continuity of the rotational transform (26) is obtained for a minimum distance  $\epsilon_{\text{SP}} \approx (1 \cdot 10^{-3} - 5 \cdot 10^{-3}) \psi_X$  on the SP side of the magnetic separatrix, but for smaller minimum distances  $\epsilon_{\text{ST}} \approx \epsilon_{\text{SC}}$

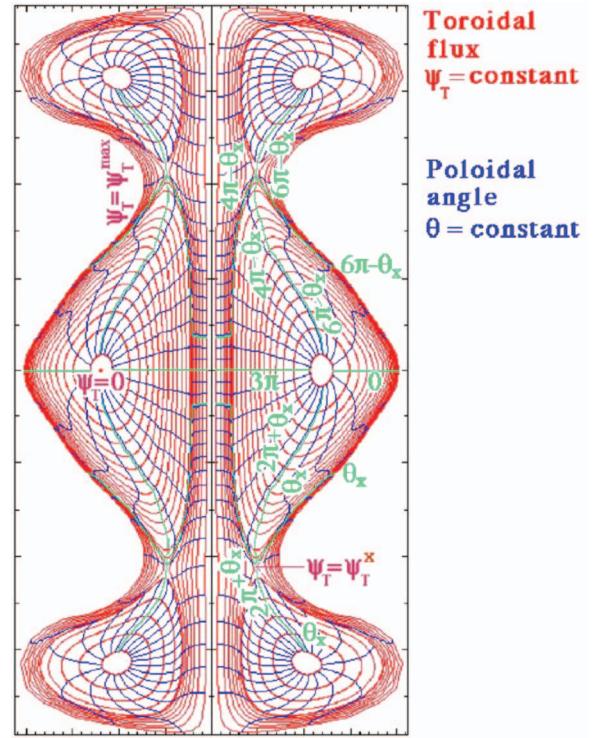


FIG. 4. (Color). Boozer radial and poloidal coordinates  $\psi_T$  (red) and  $\theta$  (blue) for the unrelaxed  $\langle \beta \rangle_{\text{ST}} = 1.02$  CKF configuration of Fig. 2. The poloidal angle label is  $3 \cdot \theta^{\text{SP}}$  inside the SP.

$\approx (2 \cdot 10^{-5} - 10^{-4}) \psi_X$  on the ST and SC side: It is, therefore, impossible to distinguish the sharp turn of the  $\theta = \text{constant}$  contours at the edge of the three tori, at such unbalanced distances from the separatrix. An example of balanced distances from the separatrix, which shows more clearly the correspondance will be discussed in Sec. VII.

In the case with up-down symmetry, the Boozer coordinates in the upper SC can be derived through mirroring rules from the calculation in the lower SC. The mirroring rules between the two SCs ( $\Delta\psi_T \leq \psi_T^{\text{SC}}$ ) have either even parity, as for

$$R(\psi_T^{\text{X}} + \psi_T^{\text{SC}} - \Delta\psi_T, 4\pi - \theta) = R(\psi_T^{\text{X}} + \psi_T^{\text{SC}} + \Delta\psi_T, \theta), \quad (28)$$

as well as for  $(\vec{\nabla}\phi \cdot \vec{\nabla}\psi_T)$ ,  $\partial\nu/\partial\theta$ ,  $\partial\nu/\partial\psi_T$  and  $B^2$ . Or they have odd parity, as for

$$\vec{\nabla}\psi_T(\psi_T^{\text{X}} + \psi_T^{\text{SC}} - \Delta\psi_T, 4\pi - \theta) = -\vec{\nabla}\psi_T(\psi_T^{\text{X}} + \psi_T^{\text{SC}} + \Delta\psi_T, \theta), \quad (29)$$

as well as for  $\vec{\nabla}\theta$ ,  $Z$ ,  $\nu$ ,  $\beta_*$ , and  $\sqrt{g}$ . The mirroring rules for the flux surface quantities between the two SCs ( $\Delta\psi_T \leq \psi_T^{\text{SC}}$ ) are, therefore,

$$\psi(\psi_T^{\text{X}} + \psi_T^{\text{SC}} - \Delta\psi_T) = \psi(\psi_T^{\text{X}} + \psi_T^{\text{SC}} + \Delta\psi_T), \quad (30)$$

$$\epsilon(\psi_T^{\text{X}} + \psi_T^{\text{SC}} - \Delta\psi_T) = \epsilon(\psi_T^{\text{X}} + \psi_T^{\text{SC}} + \Delta\psi_T), \quad (31)$$

$$I(\psi_T^{\text{X}} + \psi_T^{\text{SC}} - \Delta\psi_T) = -I(\psi_T^{\text{X}} + \psi_T^{\text{SC}} + \Delta\psi_T), \quad (32)$$

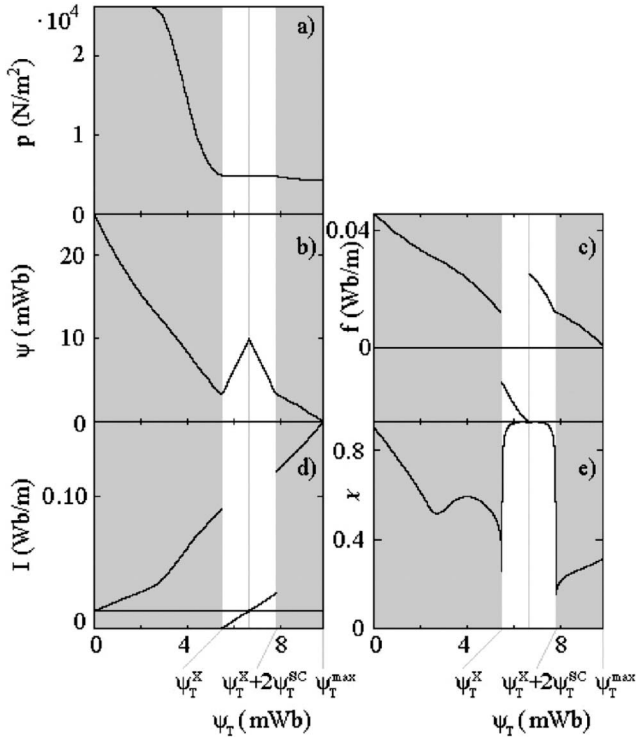


FIG. 5. Flux surface quantities for the unrelaxed  $\langle\beta\rangle_{ST}=1.02$  CKF configuration of Fig. 2, as a function of the normalized toroidal flux  $\psi_T$ : (a) kinetic pressure  $p(\psi_T)$ ; (b) poloidal flux function  $\psi(\psi_T)$ ; (c) normalized poloidal current  $f(\psi_T)$ ; (d) normalized toroidal current  $I(\psi_T)$ ; (e) rotational transform  $\epsilon(\psi_T)$ .

$$f(\psi_T^X + \psi_T^{SC} - \Delta\psi_T) = -f(\psi_T^X + \psi_T^{SC} + \Delta\psi_T). \quad (33)$$

A few of the most relevant flux surface quantities calculated for the unrelaxed CKF equilibrium, with  $\beta_{ST} = 2\mu_0\langle\rho\rangle_{ST}/\langle B^2\rangle_{ST} = 1.02$ , are shown in Fig. 5. If the up-down symmetry is removed, similar mirroring rules will apply to the innermost surrounding plasma (see Sec. III), which is run through twice, with opposite directions of  $\vec{\nabla}\psi_T$ .

## VI. METRIC COEFFICIENTS OF THE BOOZER COORDINATES AND THEIR SINGULARITIES

For the calculation of the ideal MHD stability the knowledge of the metrics coefficients<sup>20</sup>  $g_{ij} = \vec{e}_i \cdot \vec{e}_j$  is mandatory.<sup>17,18</sup> Combining the covariant expression of  $\vec{B}$  with the contravariant expressions of  $\vec{B}$  and  $\vec{\nabla}\psi_T$  the covariant basis vectors (9) are

$$\vec{e}_\psi = \frac{\vec{\nabla}\psi_T}{|\vec{\nabla}\psi_T|^2} + \frac{\beta_*}{B^2}\vec{B} - \frac{\gamma_*}{B^2}(\vec{B} \wedge \vec{\nabla}\psi_T);$$

$$\vec{e}_\theta = \frac{1}{B^2}(I\vec{B} + \vec{B} \wedge \vec{\nabla}\psi_T); \quad (34)$$

$$\vec{e}_\phi = \frac{1}{B^2}(f\vec{B} - \epsilon\vec{B} \wedge \vec{\nabla}\psi_T).$$

Note that in axisymmetry the simple relation  $\vec{e}_\phi = R\hat{e}_\phi$  con-

nects  $\vec{e}_\phi$  to the geometrical unit vector  $\hat{e}_\phi$ . However, the covariant basis vector  $\vec{e}_\psi$  contains also the term

$$\gamma_*(\psi_T, \theta) = \vec{\nabla}\psi_T \cdot (\vec{\nabla}\theta - \epsilon\vec{\nabla}\phi)/|\vec{\nabla}\psi_T|^2, \quad (35)$$

which is called ‘‘integrated residual shear.’’<sup>25</sup> It can be calculated solving the system between the two equations ( $\vec{\nabla}\psi_T \cdot \vec{\nabla}\phi = 0$ ,  $\vec{\nabla}\psi_T \cdot \vec{B} = 0$ ) and can be expressed through the difference between  $\phi$  and the geometrical azimuth  $\varphi$ ,  $\nu(\psi, \theta) = \phi - \varphi$ :

$$\gamma_*(\psi_T, \theta) = \left[ \frac{\beta_*(\epsilon\partial\nu/\partial\theta - 1) - (f + \epsilon I)\partial\nu/\partial\psi_T}{(I + f\partial\nu/\partial\theta)} \right]. \quad (36)$$

The metrics coefficients are

$$g_{\psi\psi} = \frac{1}{|\vec{\nabla}\psi_T|^2} + \frac{\beta_*^2}{B^2} + \frac{\gamma_*^2}{B^2}|\vec{\nabla}\psi_T|^2,$$

$$g_{\psi\theta} = \frac{\beta_* I}{B^2} - \frac{\gamma_*}{B^2}|\vec{\nabla}\psi_T|^2,$$

$$g_{\psi\phi} = \frac{\beta_* f}{B^2} + \epsilon \frac{\gamma_*}{B^2}|\vec{\nabla}\psi_T|^2, \quad (37)$$

$$g_{\theta\theta} = \frac{1}{B^2}(I^2 + |\vec{\nabla}\psi_T|^2), \quad g_{\theta\phi} = \frac{1}{B^2}(fI - \epsilon|\vec{\nabla}\psi_T|^2),$$

$$g_{\phi\phi} = \frac{1}{B^2}(f^2 + \epsilon^2|\vec{\nabla}\psi_T|^2).$$

The divergences of the metrics coefficients are examined for the case of CKF configurations. The first singularity to be addressed is the embedded magnetic separatrix ( $\psi_T = \psi_T^X$ ), where the rotational transform (A2) vanishes asymptotically:

$$\lim_{\psi_T \rightarrow \psi_T^X} \epsilon(\psi_T) \propto \frac{1}{|\ln|\psi_T^X - \psi_T||}, \quad (38)$$

while (13) shows that the nonorthogonality coefficient  $\beta_*(\psi_T^X, \theta)$  is regular, provided that  $(dp/d\psi)|_{\psi_X}$  is regular too. Although, for flux surfaces approaching the embedded separatrix, the Boozer poloidal angles  $\theta$  have to converge upon the regular X-points (see Appendix B), each X-point can be represented by its ‘‘central angle’’  $\theta_X$ . It is shown in Appendix A that  $|\vec{\nabla}\psi_T|^2$  at a magnetic separatrix vanishes at the X-points:

$$\lim_{\substack{\psi_T \rightarrow \psi_T^X \\ \theta \rightarrow \theta_X}} |\vec{\nabla}\psi_T|^2 \propto |\psi_T^X - \psi_T| \ln|\psi_T^X - \psi_T| \quad (39)$$

and diverges (logarithmically) far from the X-points:

$$\lim_{\substack{\psi_p \rightarrow \psi_p^X \\ |\theta - \theta_X| \rightarrow \pi/2}} |\vec{\nabla}\psi_T|^2 \propto |\ln|\psi_T^X - \psi_T||^2. \quad (40)$$

As Appendix B shows that  $\gamma_*|\vec{\nabla}\psi_T|^2$  remains regular in presence of a magnetic separatrix,  $\gamma_*(\psi_T, \theta)$  vanishes far from the X-points and diverges near the X-points:

$$\lim_{\substack{\psi_T \rightarrow \psi_T^X \\ |\theta - \theta_X| \rightarrow \pi/2}} \gamma_* \propto \frac{1}{|\ln|\psi_T^X - \psi_T||^2}, \quad (41)$$

$$\lim_{\substack{\psi_T \rightarrow \psi_T^X \\ \theta \rightarrow \theta_X}} \gamma_* \propto \frac{1}{|\psi_T^X - \psi_T| |\ln|\psi_T^X - \psi_T||}. \quad (42)$$

Therefore, the metric coefficients  $g_{\psi\psi}$ ,  $g_{\theta\theta}$ , and  $g_{\theta\psi}$  diverge near or far from the regular  $X$ -points:

$$\lim_{\substack{\psi_T \rightarrow \psi_T^X \\ \theta \rightarrow \theta_X}} g_{\psi\psi} \propto \frac{1}{|\psi_T^X - \psi_T| |\ln|\psi_T^X - \psi_T||}, \quad (43)$$

$$\lim_{\substack{\psi_T \rightarrow \psi_T^X \\ |\theta - \theta_X| \rightarrow \pi/2}} g_{\theta\theta} \propto |\ln|\psi_T^X - \psi_T||^2, \quad (44)$$

$$\lim_{\substack{\psi_T \rightarrow \psi_T^X \\ |\theta - \theta_X| \rightarrow \pi/2}} g_{\theta\psi} \propto |\ln|\psi_T^X - \psi_T||. \quad (45)$$

The second singularity to be examined is the symmetry axis ( $\psi_T = \psi_T^{\max}$  and  $R=0$ ), where  $\vec{\nabla}\psi_T$  vanishes like  $\lim_{R \rightarrow 0} |\vec{\nabla}\psi_T| \propto R$ ; it is characterized by  $f=0$  and  $\beta_* = 0$  (as  $dp/d\psi=0$ ). Therefore, only  $g_{\psi\psi}$  diverges near the symmetry axis:

$$\lim_{R \rightarrow 0} g_{\psi\psi} \propto \frac{1}{R^2}. \quad (46)$$

The third singularity is either of the two singular  $X$ -points ( $\vec{\mathbf{B}}=0$ ) on the symmetry axis, where the poloidal flux is well approximated in  $X$ -point centered local spherical coordinates ( $r, \vartheta, \varphi$ ) by a single multipole:<sup>26</sup>  $\psi \propto r^3(\sin \vartheta)^2 \cos \vartheta$ . There,  $\vec{\nabla}\psi_T$  vanishes:

$$\lim_{r \rightarrow 0} |\vec{\nabla}\psi_T| \propto r^2, \quad (47)$$

along with the magnetic field,  $\lim_{r \rightarrow 0} B \propto r$ . Appendix B shows that  $\gamma_*$  diverges:

$$\lim_{r \rightarrow 0} \gamma_*(\psi_T, \theta) \propto \left(\frac{1}{r}\right). \quad (48)$$

Also  $\sqrt{g}$ ,  $g_{\theta\theta}$ , and  $g_{\psi\psi}$  diverge near the singular  $X$ -point:

$$\lim_{r \rightarrow 0} \sqrt{g} \propto 1/r^2, \quad (49)$$

$$\lim_{r \rightarrow 0} g_{\theta\theta} \propto 1/r^2, \quad (50)$$

$$\lim_{r \rightarrow 0} g_{\psi\psi} \propto 1/r^4. \quad (51)$$

The final singularity to be considered is that of an internal magnetic axis (say  $\psi_T=0$ ), where  $\vec{\nabla}\psi_T=0$ ; only  $g_{\psi\psi}$  diverges near any magnetic axis:  $\lim_{\psi_T \rightarrow 0} g_{\psi\psi} \propto (1/|\vec{\nabla}\psi_T|^2)$ .

## VII. BOOZER COORDINATES ON THE FIRST OPEN FLUX SURFACE NEAR A MAGNETIC SEPARATRIX

Some modifications have also to be introduced in the calculation of the Boozer coordinates for an FCS plasma, like the one of PROTO-SPHERA.<sup>6</sup> The definition of the Boozer coordinates inside the force-free screw pinch, which has open flux surfaces ending upon the electrodes, is ambiguous, due to the absence of well-defined periodicities. However, the ambiguity can be removed again by the argument (see Sec. III) that, in the ideal MHD stability problem, the normal contravariant component of the perturbed plasma displacement  $\xi^{\psi}$  must be continuous between neighboring radial mesh points ( $\psi_X + \varepsilon_{ST}$ ,  $\psi_X - \varepsilon_{SP}$ ) on opposite sides of the embedded magnetic separatrix.<sup>24</sup> As the poloidal angle  $\theta^{ST}$  makes an excursion  $[\theta_X, 2\pi - \theta_X]$  upon the inboard of the spherical torus ( $\theta_X$  labeling the point with the smallest vertical coordinate upon  $\psi = \psi_X + \varepsilon_{ST}$ ), the most obvious choice is to attribute the same excursion to the poloidal angle  $\theta^{SP}$  upon the screw pinch ( $\theta_X$  labeling the point with the largest local radial coordinate upon  $\psi = \psi_X - \varepsilon_{SP}$ , near the  $X$ -point).

The field lines are in correspondence at the ST-SP interface along the embedded magnetic separatrix; this implies the continuity of the field line labels  $\theta^{ST} - \varepsilon^{ST}(\psi_T)\phi^{ST}$  and  $\theta^{SP} - \varepsilon^{SP}(\psi_T)\phi^{SP}$  between neighboring radial mesh points on opposite sides of the embedded magnetic separatrix. The correspondence between  $\theta^{SP}$  and  $\theta^{ST}$  forces the matching condition  $\varepsilon_{FCS}^{ST}(\psi_X + \varepsilon_{ST}) = \varepsilon_{FCS}^{SP}(\psi_X - \varepsilon_{SP})$  for the rotational transform. The Boozer poloidal angle is therefore fixed to  $\theta = \pi$  on the midplane of the SP and the first nonperiodical Boozer coordinate<sup>16</sup> to  $\theta_0 = \pi$ , at the geometric azimuth  $\varphi = 0$ . The continuity of the Jacobian (11) at the interface implies the continuity of  $I(\psi)$  at  $\psi = \psi_X$ . The excursion of the second nonperiodical Boozer coordinate  $\chi_0$ ,  $\Delta\chi_0 = 2\pi I(\psi)$  for one poloidal circuit, fixes  $\chi_0 = \pi I(\psi)$  on the midplane of the SP,  $\varphi = 0$ . If  $I_j$  and  $\varepsilon(\psi)$  were known, the nonperiodical coordinates  $\psi_0$  and  $\chi_0$  would be inside the SP [compare with (16) and (17) for  $\theta_0$  and  $\chi_0$  inside the ST]:

$$\theta_0(\psi, s) = \pi - \varepsilon(\psi)f(\psi) \int_s^{s_{eq}(\psi)} \frac{1}{R^2 B_p} \hat{\mathbf{e}}_p \cdot d\vec{\mathbf{l}}_p - \varepsilon(\psi)\varphi, \quad (52)$$

$$\chi_0(\psi, s) = \pi I(\psi) - \int_s^{s_{eq}(\psi)} B_p \hat{\mathbf{e}}_p \cdot d\vec{\mathbf{l}}_p + f(\psi)\varphi. \quad (53)$$

The poloidal arc-length along open flux surfaces starts with  $s=0$  on the lower electrode and reaches  $s=s_{eq}(\psi)$  on the midplane. Also the periodical Boozer angles  $\theta(\psi, s)$  and  $\phi(\psi, s)$  could be evaluated inside the SP inserting (52) and (53) into (18). The definition of  $\theta(\psi, s)$  inside the SP ( $0 \leq \psi \leq \psi_X$ ) determines  $s_0(\psi)$ , i.e., the poloidal arc-length along any open flux surfaces at which  $\theta=0$ , provided that inside the SP:

$$I(\psi) = \frac{1}{\pi} \int_{s_0(\psi)}^{s_{\text{eq}}(\psi)} B_p \hat{\mathbf{e}}_p \cdot d\vec{\mathbf{l}}_p. \quad (54)$$

It must be noted that within the SP the function  $I(\psi)$  does not anymore coincide with the normalized toroidal current  $\int \vec{\nabla} \wedge \vec{\mathbf{B}} \cdot d\vec{\mathbf{S}}_T / 2\pi$  flowing between the electrodes. The excursion<sup>16</sup> of the nonperiodical Boozer coordinate  $\theta_0$ ,  $\Delta\theta_0 = -2\pi\epsilon(\psi)$ , after one toroidal circuit, defines  $\epsilon(\psi)$  inside the SP [compare with (14) inside the ST]:

$$\epsilon(\psi) = \frac{\pi}{f(\psi) \int_{s_0(\psi)}^{s_{\text{eq}}(\psi)} \frac{1}{R^2 B_p} \hat{\mathbf{e}}_p \cdot d\vec{\mathbf{l}}_p}. \quad (55)$$

On the first open flux surface near the magnetic separatrix, the poloidal arc-length  $s_0(\psi_X - \epsilon_{\text{SP}})$  is obtained by (54):

$$I(\psi_X - \epsilon_{\text{SP}}) = \frac{1}{\pi} \int_{s_0(\psi_X - \epsilon_{\text{SP}})}^{s_{\text{eq}}(\psi_X - \epsilon_{\text{SP}})} B_p \hat{\mathbf{e}}_p \cdot d\vec{\mathbf{l}}_p = I(\psi_X + \epsilon_{\text{ST}}), \quad (56)$$

whereas  $s_0(\psi_X - \epsilon_{\text{SP}})$  corresponds to  $\theta=0$  through (55):

$$\begin{aligned} \epsilon(\psi_X - \epsilon_{\text{SP}}) &= \frac{\pi}{f(\psi_X - \epsilon_{\text{SP}}) \int_{s_0(\psi_X - \epsilon_{\text{SP}})}^{s_{\text{eq}}(\psi_X - \epsilon_{\text{SP}})} \frac{1}{R^2 B_p} \hat{\mathbf{e}}_p \cdot d\vec{\mathbf{l}}_p} \\ &= \epsilon(\psi_X + \epsilon_{\text{ST}}). \end{aligned} \quad (57)$$

For FCS configurations, if the same distance  $\epsilon_{\text{ST}} \approx (1-5) \cdot 10^{-3} \psi_X$  was used from opposite sides of the magnetic separatrix, the numerically calculated rotational transforms would be about the same:  $\epsilon_{\text{FCS}}^{\text{SP}}(\psi_X - \epsilon_{\text{ST}}) \approx \epsilon_{\text{FCS}}^{\text{ST}}(\psi_X$

$+ \epsilon_{\text{ST}}$ ); this allows for a simple iterative balanced solution  $\epsilon_{\text{ST}} \approx \epsilon_{\text{SP}}$  of the system between Eqs. (56) and (57). The lower electrode intersects the first open flux surface near the magnetic separatrix at the Boozer poloidal angle  $\theta = \theta_{\text{EL}}(\psi_X - \epsilon_{\text{SP}})$ ; the upper electrode is obviously at  $\theta = 2\pi - \theta_{\text{EL}}(\psi_X - \epsilon_{\text{SP}})$ ; for the configurations of PROTO-SPHERA, typically  $\theta_{\text{EL}}(\psi_X - \epsilon_{\text{SP}}) \approx -2$ .

## VIII. CALCULATION OF THE BOOZER COORDINATES ON ALL OPEN FLUX SURFACES

Equations (52)–(55) show that  $I(\psi)$ ,  $\epsilon(\psi)$  and, therefore, the behavior of the Boozer poloidal angle inside the SP are determined if the poloidal arc-length along the open flux surfaces  $s_0(\psi)$  is known for all the flux surfaces in the range ( $0 < \psi < \psi_X - \epsilon_{\text{SP}}$ ). The relation that determines  $s_0(\psi)$  is the equilibrium condition (12), written in terms of the poloidal flux  $\psi$ , for a force-free magnetic field:

$$df/d\psi + \epsilon dI/d\psi = 0. \quad (58)$$

When  $I(\psi)$  and  $\epsilon(\psi)$  are expressed in terms of  $s_0(\psi)$ , a first-order integro-differential equation is obtained for the unknown  $s_0(\psi)$ :

$$\frac{\partial(s_0(\psi))}{\partial\psi} = \frac{B_p(s_{\text{eq}}(\psi)) \frac{\partial s_{\text{eq}}(\psi)}{\partial\psi} + \frac{\mu_0 I_e}{2\pi\psi_X} \int_{s_0(\psi)}^{s_{\text{eq}}(\psi)} \frac{B_T}{R B_p} ds + \int_{s_0(\psi)}^{s_{\text{eq}}(\psi)} \left( \frac{\partial B_p}{\partial\psi} \right) ds}{B_p(s_0(\psi))}, \quad (59)$$

with the boundary condition  $s_0(\psi_X - \epsilon_{\text{SP}})$  on the first open flux surface, determined by the system between Eqs. (56) and (57). Equation (59) is solved iteratively: The lower electrode, far from being a single point in  $\theta$ , has a poloidal angle extent:  $\theta_{\text{EL}}(\psi) \neq \theta_{\text{EL}}(\psi_X - \epsilon_{\text{SP}})$ . On the symmetry axis ( $\psi=0$ ) the rotational transform,

$$\epsilon_{\text{symm}} = \lim_{\psi \rightarrow 0} \epsilon(\psi) = 2\pi\psi_X / [\mu_0 I_e (s_{\text{eq}}(0) - s_0(0))], \quad (60)$$

where  $s_{\text{eq}}(\psi) - s_0(\psi)$  is the distance on the symmetry axis between the midplane and the point at which  $\theta=0$ , can be calculated numerically, from (59), down to a minimum distance  $\psi = \epsilon_{\text{symm}} \approx (10^{-3} - 10^{-2}) \psi_{\text{max}}$  from the symmetry axis.

After the rotational transform  $\epsilon(\psi)$  is known inside the SP, the radial Boozer coordinate  $\psi_T$  can be extended through (5) to all open flux surfaces:

$$\psi_T = \psi_X^X - \frac{1}{2\pi} \int_{\psi_X}^{\psi} \frac{1}{\epsilon(\psi)} d\psi \quad (\text{with } \psi > \psi_X). \quad (61)$$

It must be noted that, within the SP, the radial Boozer coordinate does not anymore coincide with the normalized toroidal flux enclosed between the electrodes. The radial Boozer coordinate starts at  $\psi_T=0$  on the magnetic axis of the ST, increases to  $\psi_T = \psi_X^X$  on the separatrix and then reaches the  $\psi_T = \psi_T^{\text{max}}$  on the symmetry axis. A few of the most relevant flux surface quantities calculated for the PROTO-SPHERA configuration are shown in Fig. 6. The nonorthogonality coefficient obviously vanishes ( $\beta_* = 0$ ) inside the force-free screw pinch.

The decomposition, which allows for the mapping in cylindrical coordinates  $(R, \varphi, Z)$ , must be modified with respect to (27) to become adequate to the range of the poloidal

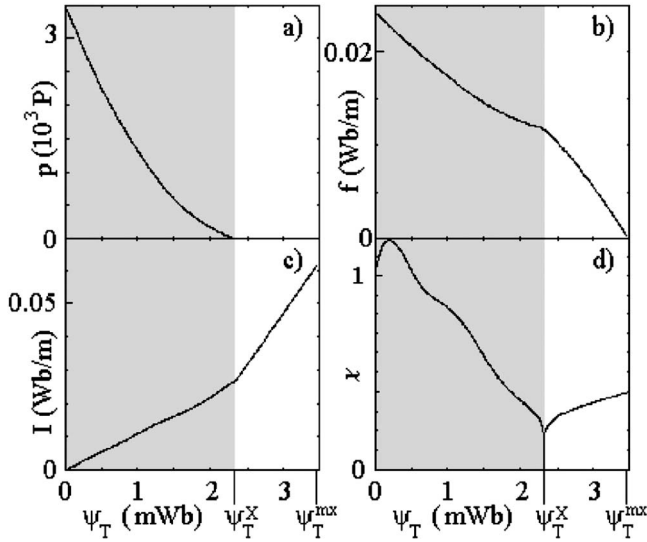


FIG. 6. Flux surface quantities for PROTO-SPHERA, with  $I_e=60$  kA,  $I_{ST}=120$  kA and  $\beta_{ST}=25\%$ , as a function of the normalized toroidal flux  $\psi_T$ : (a) kinetic pressure  $p(\psi_T)$ ; (b) normalized poloidal current  $f(\psi_T)$ ; (c) normalized toroidal current  $I(\psi_T)$ ; (d) rotational transform  $\epsilon(\psi_T)$ .

angles inside the SP, from lower to upper electrode,  $\theta \in [\theta_{EL}(\psi_T), 2\pi - \theta_{EL}(\psi_T)]$ :

$$\begin{aligned}
 R &= \sum_{j=0}^{400} \delta_j^R(\psi_T) \cos \left[ -j \left( \frac{\pi}{2[\pi - \theta_{EL}(\psi_T)]} \theta + \pi - \frac{\pi \theta_{EL}(\psi_T)}{2[\pi - \theta_{EL}(\psi_T)]} \right) \right], \\
 Z &= \sum_{j=0}^{400} \delta_j^Z(\psi_T) \cos \left[ -j \left( \frac{\pi}{2[\pi - \theta_{EL}(\psi_T)]} \theta + \pi - \frac{\pi \theta_{EL}(\psi_T)}{2[\pi - \theta_{EL}(\psi_T)]} \right) \right], \\
 \varphi &= \phi + \sum_{j=0}^{400} \delta_j^\phi(\psi_T) \cos \left[ -j \left( \frac{\pi}{2[\pi - \theta_{EL}(\psi_T)]} \theta + \pi - \frac{\pi \theta_{EL}(\psi_T)}{2[\pi - \theta_{EL}(\psi_T)]} \right) \right], \\
 B^2 &= \sum_{j=0}^{400} \delta_j^B(\psi_T) \cos \left[ -j \left( \frac{\pi}{2[\pi - \theta_{EL}(\psi_T)]} \theta + \pi - \frac{\pi \theta_{EL}(\psi_T)}{2[\pi - \theta_{EL}(\psi_T)]} \right) \right].
 \end{aligned} \tag{62}$$

The series expansion must take into account up to 200 non-zero Fourier components and the interpolation over  $\psi_T$ , with cubic splines, is based upon 20 flux surfaces (with  $\psi_T^X < \psi_T < \psi_T^{\max}$ ). The relaxation parameter  $\mu = \mu_0(\vec{j} \cdot \vec{B})/B^2$  and the vector  $\vec{\nabla}\psi_T$  are mapped in cylindrical coordinates through series expansions of the same kind. As the form (62) chosen for the mappings includes the poloidal extent of the electrodes,  $\theta_{EL}(\psi_T)$ , some complications will be introduced when

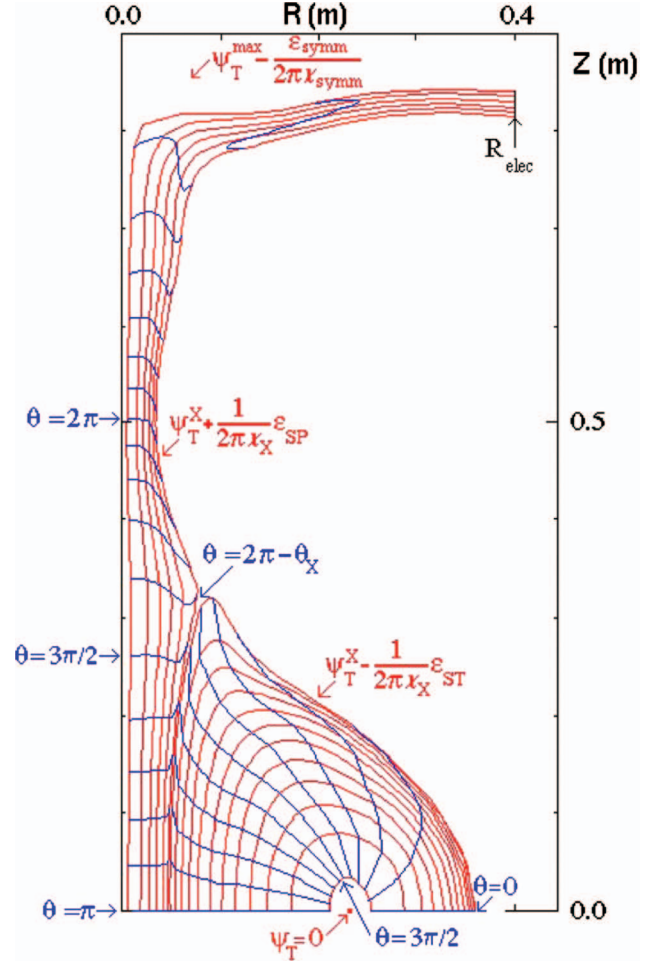


FIG. 7. (Color). Mesh of Boozer coordinates ( $\psi_T$  radial,  $\theta$  poloidal) for PROTO-SPHERA, with  $I_e=60$  kA,  $I_{ST}=120$  kA and  $\beta_{ST}=25\%$ .

the  $\partial/\partial\psi$  derivative of metrics elements has to be calculated inside the SP. The correspondence of the Boozer poloidal angle  $\theta$  shows up clearly at the ST-SP interface in the global equilibrium plot of Fig. 7, thanks to the balanced solution,  $\epsilon_{ST} \approx \epsilon_{SP}$ , of the system between Eqs. (56) and (57).

The accuracy of the calculation of the Boozer coordinates has been thoroughly checked both on closed as well as on open flux surfaces. The quantities  $R$ ,  $\varphi$ ,  $Z$ , and  $B^2$  determined by the mappings (27) and (62) along the field line  $\theta_0 = \theta - \epsilon\phi = 0$  (starting from  $\theta=0$  at the azimuth  $\varphi=0$ ) have been compared with the same quantities determined by an independent field line tracing calculation, purely based upon the value of the equilibrium field  $\vec{B}$  and starting at the same position ( $\theta=0$ ,  $\varphi=0$ ). Furthermore Appendix C shows that, after the Boozer coordinates have been calculated, the averaged part of the equilibrium condition (12) can reveal the inaccuracies of the equilibrium solver as well as those of the magnetic coordinate evaluation.

## IX. SUMMARY

The purpose of this paper is threefold: The first task is that of calculating the magnetic (Boozer) coordinates for a general CKF configuration, which embeds a magnetic separatrix connecting multiple tori (doubly connected plasma re-

gions with magnetic surfaces closed around a single magnetic axis), while the outermost surrounding plasma has the topology of a toroidal shell, extending up to the symmetry axis and carved by a number of toroidal regions. The radial coordinate  $\psi_T$  (normalized toroidal flux) is correctly ordered by alternating the direction of its gradient: For an odd number of tori,  $\vec{\nabla}\psi_T$  starts ( $\psi_T=0$ ) pointing out from the magnetic axis of the first torus toward the magnetic separatrix, then points out of the magnetic separatrix toward the magnetic axis of the second torus, thereafter it jumps to the magnetic axis of the third torus and so on and so forth for the remaining tori, until the toroidal shell surrounding plasma is reached and the maximum value of the radial coordinate ( $\psi_T=\psi_T^{\text{max}}$ ) is given to the plasma edge and to the symmetry axis. The requirement of continuity with the main torus, at the embedded magnetic separatrix, fixes the additive constants on  $\theta$ ,  $\varphi$ , and  $\beta_*(\psi_T, \theta)$  inside the secondary tori.

As far as the ideal MHD stability calculation is concerned, the normal contravariant component of the perturbed plasma displacement  $\xi^\psi$  must be continuous at all interfaces; this establishes a correspondence between the poloidal angle  $\theta$  at the edge of the three tori and the poloidal angle  $3 \cdot \theta$  at the edge of the surrounding plasma. Furthermore, as the field lines correspond along the embedded magnetic separatrix, the rotational transform  $\epsilon$  has to obey a matching condition. Near the separatrix  $\epsilon$  exhibits a vanishing logarithmic behavior in terms of the poloidal flux  $\psi$ ,  $\lim_{\psi \rightarrow \psi_X} \epsilon(\psi) = -A/\ln|C(\psi - \psi_X)|$ . The two coefficients  $A$  and  $C$  can be found by a fitting procedure down to the minimum distance from the magnetic separatrix where  $\epsilon(\psi)$  can still be calculated numerically. For CKF configurations, the  $\xi^\psi$  continuity and the  $\epsilon$  matching condition provide adjacent radial mesh points on opposite sides of the separatrix: At a distance  $\epsilon_{\text{SP}} \approx (1 \cdot 10^{-3} - 5 \cdot 10^{-3})\psi_X$  on the side of the surrounding discharge and at smaller distances  $\epsilon_{\text{ST}} \approx \epsilon_{\text{SC}} \approx (2 \cdot 10^{-5} - 10^{-4})\psi_X$  on the side of the tori.

The second task of this paper is that of analyzing in detail all the possible divergences of the quantities relevant to the calculation of the ideal MHD stability of an axisymmetric plasma, in presence of magnetic separatrices:

- At the embedded magnetic separatrix ( $\psi_T = \psi_T^X$ ), the divergences are, near the regular X-points:

$$\lim_{\substack{\psi_T \rightarrow \psi_T^X \\ \theta \rightarrow \theta_X}} g_{\psi\psi} \propto 1/|\psi_T^X - \psi_T| |\ln|\psi_T^X - \psi_T||$$

and

$$\lim_{\substack{\psi_T \rightarrow \psi_T^X \\ \theta \rightarrow \theta_X}} \gamma_* \propto 1/|\psi_T^X - \psi_T| |\ln|\psi_T^X - \psi_T||;$$

far from the regular X-point:

$$\lim_{\substack{\psi_T \rightarrow \psi_T^X \\ |\theta - \theta_X| \rightarrow \pi/2}} g_{\theta\theta} \propto |\ln|\psi_T^X - \psi_T||^2$$

and

$$\lim_{\substack{\psi_T \rightarrow \psi_T^X \\ |\theta - \theta_X| \rightarrow \pi/2}} g_{\theta\varphi} \propto |\ln|\psi_T^X - \psi_T||.$$

- At the plasma edge, near the singular X-points:

$$\lim_{\substack{\psi_T \rightarrow \psi_T^{\text{max}} \\ \theta \rightarrow \theta_{B=0}}} g_{\psi\psi} \propto 1/r^4,$$

$$\lim_{\substack{\psi_T \rightarrow \psi_T^{\text{max}} \\ \theta \rightarrow \theta_{B=0}}} \sqrt{g} \propto 1/r^2, \quad \lim_{\substack{\psi_T \rightarrow \psi_T^{\text{max}} \\ \theta \rightarrow \theta_{B=0}}} g_{\theta\theta} \propto 1/r^2,$$

and

$$\lim_{\substack{\psi_T \rightarrow \psi_T^{\text{max}} \\ \theta \rightarrow \theta_{B=0}}} \gamma_*(\psi_T, \theta) \propto (1/r),$$

where  $r$  is the distance from the singular X-point.

The third task of this paper is that of calculating the Boozer coordinates for FCS configurations, which are characterized by closed flux surfaces (spherical torus) and open flux surfaces ending upon electrodes (screw pinch), connected by a magnetic separatrix. Again, the continuity of the perturbed plasma displacement  $\xi^\psi$  and the matching conditions for the field lines at the magnetic separatrix ( $\psi = \psi_X$ ) remove the ambiguities in the definitions of magnetic coordinates on the open flux surfaces. On any open flux surface  $\psi$ , the normalized toroidal current  $I(\psi)$  and the rotational transform  $\epsilon(\psi)$  are expressible by line integrals along the poloidal arc-length, with a lower integration boundary  $s_0(\psi)$ . The equilibrium relation for a force-free magnetic field,  $df/d\psi + \epsilon dI/d\psi = 0$ , determines  $s_0(\psi)$  for every open flux surface. After  $\epsilon(\psi)$  is known, the definition of the radial Boozer coordinate  $\psi_T$  is extended to all open flux surfaces; however, neither  $\psi_T$  nor  $I(\psi)$  do coincide, respectively, with the normalized toroidal flux and with the normalized toroidal current flowing between the electrodes. For FCS configurations, the  $\xi^\psi$  continuity and the  $\epsilon$  matching condition provide two adjacent radial mesh points on opposite sides of the separatrix, both at a distance  $|\psi - \psi_X| \approx (1-5) \cdot 10^{-3} \psi_X$ .

## APPENDIX A: ROTATIONAL TRANSFORM NEAR THE EMBEDDED SEPARATRIX

In an axisymmetric magnetic configuration, the rotational transform  $\epsilon$  is evaluated, upon the poloidal cross-section of any flux surface, by the contour integral (14); it vanishes at a magnetic separatrix with regular X-points (where  $B_p=0$ , but  $\vec{B} \neq 0$ ):  $\epsilon(\psi_T^X)=0$ , in terms of the normalized toroidal flux  $\psi_T = \psi_T^X$ , or as  $\epsilon(\psi_X)=0$ , in terms of the poloidal flux  $\psi = \psi_X$  enclosed within the magnetic separatrix. A two wires analytical field model, derived from a 2D conformal complex potential, shows that near a separatrix with regular X-points:

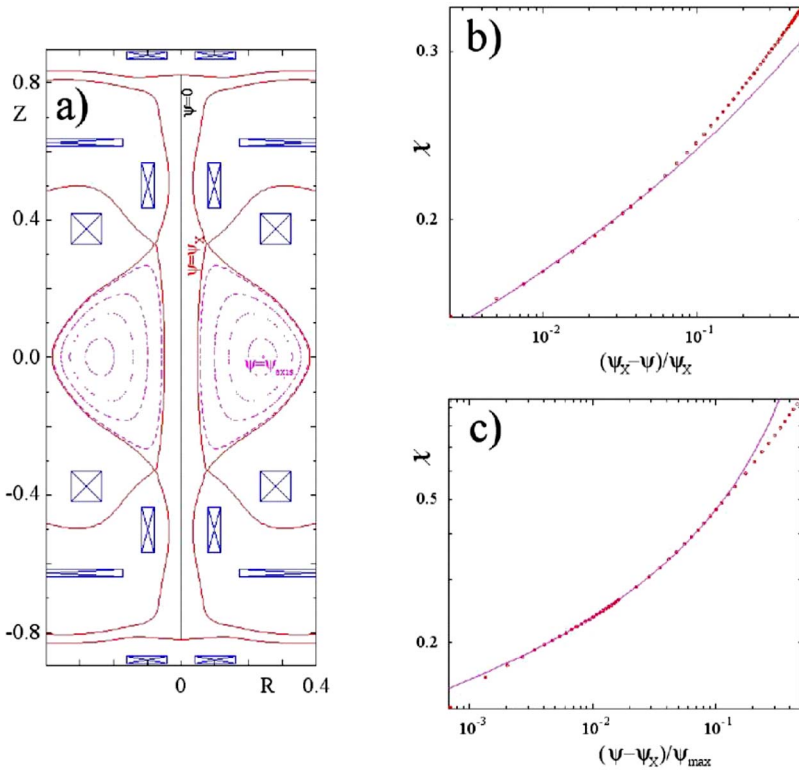


FIG. 8. (Color online). PROTO-SPHERA equilibrium, calculated by finite element method solver, with  $\beta = 0.25$ ,  $I_{ST}/f=2.0$ , normalized currents  $I_{ST} = 2.4 \cdot 10^{-2}$  T·m,  $f=1.2 \cdot 10^{-2}$  T·m, angle between separatrix tails  $55^\circ$ , distance of the X-point from the symmetry axis  $R_X=0.077$  m, poloidal flux on the magnetic axis  $\psi_{max}=1.31 \cdot 10^{-2}$  Wb and at the separatrix  $\psi_X = 2.32 \cdot 10^{-3}$  Wb. (a) Flux surfaces. (b) Behavior of  $\log_{10}[\epsilon(\psi)]$  in the SP fitted by  $\epsilon(\psi) = -1.6/\ln[5.07 \cdot (\psi - \psi_X)]$ , normalized distance from the magnetic separatrix  $\log_{10}[(\psi_X - \psi)/\psi_X]$ . (c) Behavior of  $\log_{10}[\epsilon(\psi)]$  in the ST fitted by  $\epsilon(\psi) = -1.09/\ln[7.35 \cdot 10^1(\psi - \psi_X)]$ , normalized distance from the magnetic separatrix  $\log_{10}[(\psi - \psi_X)/\psi_{max}]$ .

$$\lim_{\psi \rightarrow \psi_X} \epsilon(\psi) = -A \frac{1}{\ln|C(\psi - \psi_X)|}, \quad (\text{A1})$$

even when the presence of a nonvanishing toroidal plasma current density ( $j_\phi \neq 0$ ) upon the X-points imposes a nonorthogonal crossing of the separatrix tails.

For a numerical equilibrium the two coefficients  $A$  and  $C$  can be found by a fitting procedure. As an example, the numerical behavior of  $\epsilon(\psi)$  for an FCS equilibrium<sup>13</sup> can be explored down to a distance  $|\psi - \psi_X| \approx 2 \cdot 10^{-3} \psi_{max}$  from the magnetic separatrix (see Fig. 8).

Integrating (A1),  $\epsilon(\psi_T)$  vanishes asymptotically as

$$\lim_{\psi \rightarrow \psi_T^X} \epsilon(\psi_T) \propto -\frac{1}{\ln(\psi_T^X - \psi_T)}, \quad (\text{A2})$$

while its radial derivative diverges as

$$\lim_{\psi \rightarrow \psi_T^X} \frac{d\epsilon}{d\psi_T} \propto -\frac{1}{(\psi_T^X - \psi_T) \ln^2(\psi_T^X - \psi_T)}. \quad (\text{A3})$$

At a magnetic separatrix  $|\vec{\nabla}\psi|$  varies: Near the X-point it vanishes like  $|\vec{\nabla}\psi| \propto \rho$ , where  $\rho$  is the local distance from the X-point; far from the X-point  $|\vec{\nabla}\psi| = RB_\rho/2\pi$  is regular and finite. The two wires analytical field model shows that the squared gradient  $|\vec{\nabla}\psi_T|^2$  has the following asymptotic limits:

$$\lim_{\substack{\psi_T \rightarrow \psi_T^X \\ \theta \rightarrow \theta_X}} |\vec{\nabla}\psi_T|^2 \propto |\psi_T^X - \psi_T| |\ln|\psi_T^X - \psi_T||; \quad (\text{A4})$$

$$\lim_{\substack{\psi_T \rightarrow \psi_T^X \\ |\theta - \theta_X| \rightarrow \pi/2}} |\vec{\nabla}\psi_T|^2 \propto |\ln|\psi_T^X - \psi_T||^2, \quad (\text{A5})$$

respectively, near and far from a regular X-point, represented by its ‘‘central poloidal angle’’  $\theta_X$  (see Appendix B).

## APPENDIX B: INTEGRATED RESIDUAL SHEAR NEAR THE EMBEDDED SEPARATRIX

Given the asymptotic limit (A4) for  $|\vec{\nabla}\psi_T|^2$ , the components of  $\vec{\nabla}\theta$  and  $\vec{\nabla}\phi$  upon the flux surfaces diverge near the regular X-point like

$$\lim_{\substack{\psi_T \rightarrow \psi_T^X \\ \theta \rightarrow \theta_X}} \left( \frac{|\vec{\nabla}\theta \wedge \vec{\nabla}\psi_T|}{|\vec{\nabla}\psi_T|}, \frac{|\vec{\nabla}\phi \wedge \vec{\nabla}\psi_T|}{|\vec{\nabla}\psi_T|} \right) \propto \lim_{\substack{\psi_T \rightarrow \psi_T^X \\ \theta \rightarrow \theta_X}} \frac{1}{|\vec{\nabla}\psi_T|} \propto \frac{1}{\sqrt{|\psi_T^X - \psi_T|} \sqrt{|\ln|\psi_T^X - \psi_T||}}. \quad (\text{B1})$$

This relation for  $\vec{\nabla}\theta$  shows that for flux surfaces approaching the separatrix the Boozer poloidal angles have to converge upon the regular X-points. Nevertheless, each X-point can be represented by its ‘‘central angle’’  $\theta_X$ . Such angle corresponds to the limit of the Boozer poloidal angle on the innermost SP magnetic surface tracing the local (near the regular X-point) maximum distance from the symmetry axis, while approaching the magnetic separatrix (see Fig. 7). On the magnetic separatrix, but far from the X-point, taking the appropriate asymptotic limits for the covariant basis vectors  $\vec{e}_\theta$  and  $\vec{e}_\phi$

(34), the component of  $\vec{\nabla}\theta$  upon the flux surfaces vanishes like

$$\lim_{\substack{\psi_T \rightarrow \psi_T^X \\ |\theta - \theta_X| \rightarrow \pi/2}} \frac{|\vec{\nabla}\theta \wedge \vec{\nabla}\psi_T|}{|\vec{\nabla}\psi_T|} \propto \lim_{\substack{\psi_T \rightarrow \psi_T^X \\ |\theta - \theta_X| \rightarrow \pi/2}} \frac{1}{|\vec{\nabla}\psi_T|} \propto \frac{1}{|\ln|\psi_T^X - \psi_T||}, \quad (B2)$$

whereas the component of  $\vec{\nabla}\phi$  upon the flux surfaces is regular.

Equation (36) expresses the integrated residual shear  $\gamma_*(\psi_T, \theta)$  in terms of the difference  $\nu(\psi_T, \theta) = \phi - \varphi$  between the Boozer toroidal angle  $\phi$  and the geometrical azimuth  $\varphi$ . The calculation of  $\gamma_*(\psi_T, \theta)$  meets, however, a numerical difficulty at the regular X-points of the configuration: The system between the two equations  $(\vec{\nabla}\psi_T \cdot \vec{\nabla}\phi) = 0$  and  $(\vec{\nabla}\psi_T \cdot \vec{B}) = 0$  becomes indeterminate, as  $\vec{B} \propto \vec{\nabla}\phi$  at the regular X-points. However, dotting the covariant basis vector  $\vec{e}_\phi$  (34), respectively, with it  $\vec{e}_\theta$  and  $\vec{e}_\psi$ , and neglecting  $\epsilon^2|\vec{\nabla}\psi_T|^2$  with respect to  $f^2$  it is possible to show that  $\lim_{\psi_T \rightarrow \psi_T^X} \partial(\gamma_*|\vec{\nabla}\psi_T|^2)/\partial\theta|_{\theta_X} = 0$ ; which means that, on a given surface near the separatrix,  $\gamma_*|\vec{\nabla}\psi_T|^2$  is constant in a range of poloidal angles around  $\theta = \theta_X$ . Therefore,  $\gamma_*(\psi_T, \theta)$  can diverge at the regular X-point not faster than

$$\lim_{\substack{\psi_T \rightarrow \psi_T^X \\ \theta \rightarrow \theta_X}} \gamma_* \leq O\left(\frac{1}{|\psi_T^X - \psi_T| |\ln|\psi_T^X - \psi_T||}\right). \quad (B3)$$

From the identity  $(\vec{\nabla}\theta - \epsilon\vec{\nabla}\phi) = (\vec{B} \wedge \vec{\nabla}\psi_T)/|\vec{\nabla}\psi_T|^2 + \gamma_*\vec{\nabla}\psi_T$ , using (B2) and (A5), it turns out that  $\gamma_*(\psi_T, \theta)$  vanishes far from the regular X-point:

$$\lim_{\substack{\psi_T \rightarrow \psi_T^X \\ |\theta - \theta_X| \rightarrow \pi/2}} \gamma_* \leq o\left(\frac{1}{|\ln|\psi_T^X - \psi_T||^2}\right). \quad (B4)$$

The asymptotic limit of the integrated residual shear  $\gamma_*(\psi_T, \theta)$  at the singular X-points on the symmetry axis ( $R = 0$ ) remains to be investigated. Given the expression (34) of the covariant basis vector  $\vec{e}_\phi$  and the asymptotic limit  $\lim_{r \rightarrow 0} |\vec{\nabla}\psi_T| \propto r^2$ , the component of  $\vec{\nabla}\theta$  upon the flux surfaces, vanishes near the singular X-point like

$$\lim_{r \rightarrow 0} |\vec{\nabla}\theta \wedge \vec{\nabla}\psi_T|/|\vec{\nabla}\psi_T| \propto r, \quad (B5)$$

where  $r$  is the distance from the singular X-point. This explains why no convergence of poloidal Boozer angles  $\theta$  oc-

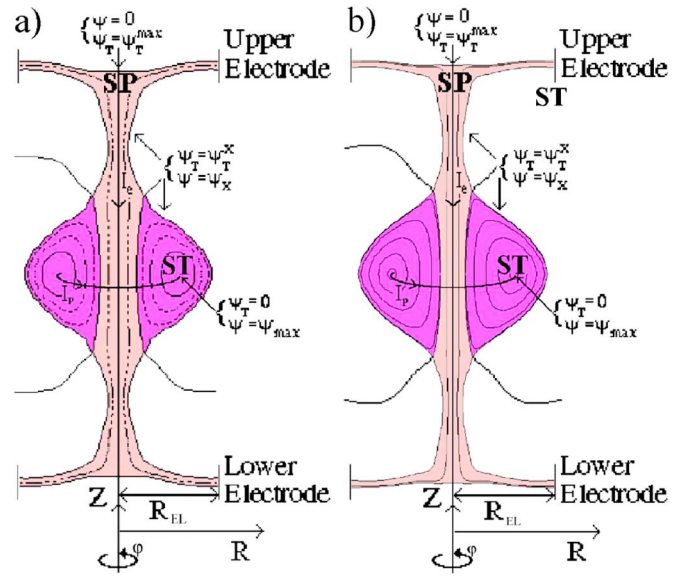


FIG. 9. (Color online). Equilibrium solution for the combined open and closed flux surfaces of PROTO-SPHERA, with  $I_e = 60$  kA,  $I_{ST} = 120$  kA and  $\beta_{ST} = 25\%$ : (a) spherical multipolar code; (b) finite element code.

cur at the singular X-point on the symmetry axis (see Figs. 4 and 7), which is therefore uniquely characterized by the poloidal angle  $\theta = \theta_{B=0}$ . The angle  $\theta_{B=0}$  is defined in the numerical calculation as the poloidal angle which labels the point where  $B$  reaches its minimum value, on the outermost numerical SP magnetic surface  $\psi = \epsilon_{\text{symm}}$ . Finally the integrated residual shear  $\gamma_*(\psi_T, \theta)$  can diverge at the singular X-point not faster than

$$\lim_{\substack{\psi_T \rightarrow \psi_T^{\text{max}} \\ \theta \rightarrow \theta_{B=0}}} \gamma_*(\psi_T, \theta) \leq o\left(\frac{1}{r}\right). \quad (B6)$$

### APPENDIX C: NUMERICAL ACCURACY OF EQUILIBRIUM CALCULATIONS AND OF BOOZER COORDINATE EVALUATION

Figure 9 compares the equilibrium solutions for the combined closed and open flux surfaces of a FCS configuration (PROTO-SPHERA), calculated, respectively, with a spherical multipolar and with a finite element code. As the averaged part of the equilibrium condition (12) is

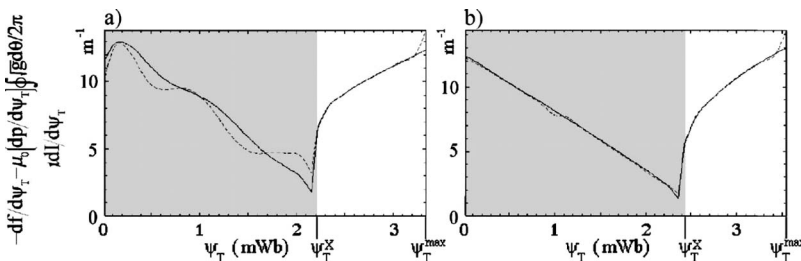


FIG. 10. Boozer coordinate analysis for the PROTO-SPHERA equilibrium solutions of Fig. 9, with  $I_e = 60$  kA,  $I_{ST} = 120$  kA and  $\beta_{ST} = 25\%$ . Averaged equilibrium components  $-df/d\psi_T - \mu_0(dp/d\psi_T)\sqrt{gd\theta}/2\pi$  (full line) and  $\epsilon dl/d\psi_T$  (dotted line), as a function of  $\psi_T$ : (a) spherical multipolar code; (b) finite element code.

$$-df/d\psi_T - \mu_0(dp/d\psi_T) \oint \sqrt{gd}\theta/2\pi = \epsilon l/d\psi_T. \quad (C1)$$

Once the Boozer coordinates have been calculated, the comparison between the two terms of this equation reveals the inaccuracies of both the equilibrium solver as well as of the coordinate evaluation. The matching of the two sides of (C1) shown in Fig. 10(a) for the spherical multipolar equilibrium solver is indeed less accurate in the low-pressure region at the edge of the spherical torus ( $\psi_T \leq \psi_T^X$ ). This is due to the large number of spherical multipolar moments<sup>12</sup> ( $N_{\max} = 40 \div 50$ ) that must be accounted for, in order to obtain a correct description of the narrowest part of the screw pinch. However, such inaccuracies do lead only to minor changes in the growth rates of the ideal MHD instabilities. Figure 10(b) shows that for the finite element equilibrium calculations the matching of the averaged part of the equilibrium condition (C1) is instead very good. Some inaccuracies with the calculation of  $I(\psi)$  and  $\epsilon(\psi)$ , through the first-order integro-differential equation (59), still remain near the symmetry axis ( $\psi_T = \psi_T^{\max}$ ).

<sup>1</sup>Y.-K. M. Peng and D. J. Strickler, Nucl. Fusion **26**, 1139 (1986).

<sup>2</sup>A. Sykes, E. Del Bosco, R. J. Colchin, G. Cunningham, R. Duck, T. Edlington, D. H. J. Goodall, M. P. Gryaznevich, J. Holt, J. Hugill, J. Li, S. J. Manhood, B. J. Parham, D. C. Robinson, T. N. Todd, and M. F. Turner, Nucl. Fusion **32**, 694 (1992).

<sup>3</sup>A. Sykes, R. J. Akers, L. C. Appel, E. R. Arends, P. G. Carolan, N. J. Conway, G. F. Counsell, G. Cunningham, A. Dnestrovskij, Yu. N. Dnestrovskij, A. R. Field, S. J. Fielding, M. P. Gryaznevich, S. Korsholm, E. Laird, R. Martin, M. P. S. Nightingale, C. M. Roach, M. R. Tournianski, M. J. Walsh, C. D. Warrick, H. R. Wilson, S. You, MAST Team, and NBI Team, Nucl. Fusion **41**, 1423 (2001).

<sup>4</sup>M. Ono, S. M. Kaye, Y.-K. M. Peng, G. Barnes, W. Blanchard, M. D. Carter, J. Chrzanowski, L. Dudek, R. Ewig, D. Gates, R. E. Hatcher, T. Jarboe, S. C. Jardin, D. Johnson, R. Kaita, M. Kalish, C. E. Kessel, H. W. Kugel, R. Maingi, R. Majeski, J. Manickam, B. McCormack, J. Menard, D. Mueller, B. A. Nelson, B. E. Nelson, C. Neumeyer, G. Oliaro, F. Paoletti, R. Parsells, E. Pery, N. Pomphrey, S. Ramakrishnan, R. Raman, G. Rewoldt, J. Robinson, A. L. Roquemore, P. Ryan, S. Sabbagh, D. Swain, E. J. Synakowski, M. Viola, M. Williams, J. R. Wilson, and NSTX Team, Nucl. Fusion **40**, 557 (2000).

<sup>5</sup>M. Yamada, N. Pomphrey, A. Morita, Y. Ono, and M. Katsurai, Nucl.

Fusion **36**, 1210 (1996).

<sup>6</sup>F. Alladio, A. Mancuso, P. Micozzi, L. Pieroni, C. Alessandrini, G. Apruzzese, L. Bettinali, P. Buratti, A. Coletti, P. Costa, C. Crescenzi, A. Cucchiari, R. De Angelis, T. Fortunato, D. Frigione, M. Gasparotto, G. Gatti, R. Giovagnoli, L. A. Grosso, G. Maddaluno, G. Maffia, S. Mantovani, G. Monari, C. Nardi, S. Papastergiou, M. Pillon, A. Pizzuto, M. Roccella, F. Rogier, M. Santinelli, L. Semeraro, A. Sibio, B. Tilia, O. Tudisco, L. Zannelli, and V. Zanza, *PROTO-SPHERA*, ENEA, Serie Energia, Associazione Euratom-ENEA sulla Fusione, RT/ERG/FUS/2001/14 (2001), ISSN 1124/7932.

<sup>7</sup>T. H. Jensen and M. S. Chu, J. Plasma Phys. **25**, 459 (1980).

<sup>8</sup>J. B. Taylor and M. F. Turner, Nucl. Fusion **29**, 219 (1989).

<sup>9</sup>M. Nagata, T. Kanki, T. Masuda, S. Naito, H. Tatsumi, and T. Uyama, Phys. Rev. Lett. **71**, 4342 (1993).

<sup>10</sup>N. Amemiya, A. Morita, and M. Katsurai, J. Phys. Soc. Jpn. **63**, 1552 (1993).

<sup>11</sup>F. Rogier, G. Bracco, A. Mancuso, P. Micozzi, and F. Alladio, *Proceedings of 11th International Congress on Plasma Physics*, ICPP 2002, Sydney, 2002, edited by I. S. Falconer, R. L. Dewar, and J. Khachan (American Institute of Physics, Melville NY, 2003), Vol. 669, p. 557.

<sup>12</sup>F. Alladio and P. Micozzi, Nucl. Fusion **37**, 1759 (1997).

<sup>13</sup>F. Rogier and A. Mancuso, Int. J. Comput. Eng. Sci. **5**, 1 (2004).

<sup>14</sup>I. B. Bernstein, E. A. Frieman, M. D. Kruskal, and R. M. Kulsrud, Proc. R. Soc. London, Ser. A **244**, 17 (1958).

<sup>15</sup>L. Degtyarev, A. Martynov, S. Medvedev, F. Troyon, L. Villard, and R. Gruber, Comput. Phys. Commun. **103**, 10 (1997).

<sup>16</sup>A. H. Boozer, Phys. Fluids **24**, 1999 (1981).

<sup>17</sup>J. Nührenberg and R. Zille, in *Proceedings of the Workshop on Theory of Fusion Plasmas*, EUR 11336 EN (Editrice Compositori, Bologna, 1987), p. 3.

<sup>18</sup>W. A. Cooper, Plasma Phys. Controlled Fusion **34**, 1011 (1992).

<sup>19</sup>D. V. Antonsen, W. A. Cooper, R. Gruber, S. Merazzi, and U. Schwenn, Int. J. Supercomput. Appl. **4**, 34 (1990).

<sup>20</sup>W. D. D'haeseleer, W. N. G. Hitchon, J. D. Callen, and J. L. Shohet, *Flux Coordinates and Magnetic Field Structure* (Springer-Verlag, Berlin, 1991), pp. 7–39.

<sup>21</sup>P. C. Grim, J. M. Greene, and J. L. Johnson, in *Methods in Computational Physics* (Academic, New York, 1976), Vol. 16, p. 253.

<sup>22</sup>S. Hamada, Nucl. Fusion **2**, 23 (1962).

<sup>23</sup>C. Mercier, *Lectures in Plasma Physics*, EUR 5127 EN/1987 (Commission of the European Communities, Luxembourg, 1987), p. 19.

<sup>24</sup>R. Gruber and J. Rappaz, *Finite Element Methods in Linear Ideal Magnetohydrodynamics* (Springer-Verlag, Berlin, 1985), p. 39.

<sup>25</sup>A. Pletzer, A. Bondeson, and R. L. Dewar, J. Comput. Phys. **115**, 530 (1994).

<sup>26</sup>P. M. Morse and H. Feshbach, *Methods of Theoretical Physics* (McGraw-Hill, New York, 1953), p. 1264.